Journal of Electroanalytical Chemistry 862 (2020) 113969

Contents lists available at ScienceDirect

Journal of Electroanalytical Chemistry

journal homepage: www.elsevier.com/locate/jelechem

Double imprinting-based electrochemical detection of mimetic exosomes

Yuyuan Zhu, Yu An, Rui Li, Fan Zhang *, Qingjiang Wang *, Pingang He

School of Chemistry and Molecular Engineering, East China Normal University, 500 Dongchuan Road, Shanghai 200241, PR China

ARTICLE INFO

Article history:
Received 19 November 2019
Received in revised form 27 January 2020
Accepted 17 February 2020
Available online 19 February 2020

Keywords:
Double-imprinting
Particle size distribution
Mimetic exosomes
Electrochemical sensing

ABSTRACT

Exosomes (30–150 nm) secreted by cells play an important role in intercellular communication. Herein, a novel double imprinting-based electrochemical method has been developed for analyzing the particle size distribution (PSD) of mimetic exosomes – a mixture of SiO_2@HRP with the diameters in 50 nm, 100 nm and 150 nm at a ratio similar to the exosomes. Double imprinting polymers (DIP) were synthesized with SiO_2@HRP at different sizes as template, providing the both recognition of size and morphology. With the capture of the target and the binding of the signal amplification tag – SiO_2@Ag/MPBA on the DIP film, a sandwich structure was constructed on Au NPs-GO modified glassy carbon electrode. Under the optimal conditions, the DIP film exhibits the linear correlations between the current intensity and the logarithmic concentration of SiO_2@HRP as $\Delta I_{50} = -1.52 + 0.50 \times \lg c_{50}$ (2.89×10^4–2.89×10^9 particles/mL), $\Delta I_{100} = -1.61 + 0.48 \times \lg c_{100}$ (2.89×10^4–2.89×10^9 particles/mL) and $\Delta I_{150} = -1.54 + 0.49 \times \lg c_{150}$ (5.75×10^4–5.75×10^9 particles/mL) with the limit of detection of 1.44×10^3 particles/mL, 5.68×10^2 particles/mL and 7.70×10^2 particles/mL, respectively. Furthermore, the DIP film was applied to the PSD analysis of mimetic exosomes – SiO_2@HRP at mixed sizes with a ratio of 50 nm:100 nm:150 nm = 5.0%:42.5%:52.5% detected by nanoparticle tracking analysis (NTA), obtaining a similar result of 50 nm:100 nm:150 nm = 3.6%:43.0%:53.4% with small relative concentration errors. It also exhibited excellent reproducibility and stability. This double imprinting-based method shows high potential in the separation and detection of complex biosamples.

© 2020 Elsevier B.V. All rights reserved.

1. Introduction

Exosomes and microvesicles are released by cells into their environment as submicron particles with different sizes [1,2]. Surface glycoconjugates derived from mother cells make these vesicles play an important role in many biological processes and are closely related to diseases, such as cancer and retrovirus infection [3–5].

Owing to small size, highly heterogeneous and the low refractive index of the above microparticles, it is extremely challenging to detect them with conventional detection methods. The particle size distribution (PSD) defines the size as a function of concentration, preferably refers to the number of vesicles in a unit suspension volume [6]. Current feasible and potential methods for the characterization and detection of exosomes include transmission electron microscope (TEM) [7,8], nanoparticle tracking analysis (NTA) [9–13], dynamic light scattering (DLS) [14], and atomic force microscope (AFM) [15], and flow cytometry (FC) [16–18]. However, most of them require skilled operation [8,17,18] and expensive equipment. It is hard to obtain PSD information and quantify simultaneously [8,15], and susceptible to the interference [19].

Molecularly imprinted polymers (MIPs), are copolymerized with the template, monomers and crosslinkers in the presence of initiators. Superior chemical stability, heat resistance, solvent resistance and low costs make the molecular imprinting technique widely used in artificial receptors [20–24]. Its superior selective recognition to the target based on the high matching of the imprinted cavity with the template provides a new way to analyze particle size distribution (PSD) of exosomes [25,26]. But it is still challenging. There are lots of proteins on the exosomes surface and some particles with similar size and shape would interfere the detection of exosomes [27,28]. Thus, it is hard to recognize exosomes only depending on the size and shape. Therefore, the double recognition of the target by both the size and morphology (including the shape and surface ultrastructure) is in high demand for increasing the affinity between the imprinting film and the target, and the recognition efficiency.

Herein, double imprinting-based electrochemical detection strategy has been developed for analyzing the particle size distribution of mimetic exosomes, relying on the both size and morphology of the nanoparticles. The mixture of silica nanoparticles (SiO_2 NPs) wrapped by the glycoprotein – horseradish peroxidase (HRP) with the diameters in 50 nm, 100 nm and 150 nm at a ratio similar to the exosomes was employed as mimetic exosomes (SiO_2@HRP for short). The double imprinting polymers were formed on the gold nanoparticles and reduced graphene oxide (Au NPs-GO) modified glassy carbon electrode, using methacrylic acid (MAA) and

* Corresponding authors.
E-mail addresses: fzhang@chem.ecnu.edu.cn, (F. Zhang), qjwang@chem.ecnu.edu.cn. (Q. Wang).

http://dx.doi.org/10.1016/j.jelechem.2020.113969
1572-6657/© 2020 Elsevier B.V. All rights reserved.

4-vinylphenylboronic (VPBA) as monomers and SiO_2@HRP at different sizes as template. After rebinding the target – SiO_2@HRP, the signal amplification tag – SiO_2@Ag/MPBA was bound to SiO_2@HRP by the formation of boric acid ester between 4-mercaptophenylboronic acid (MPBA) and HRP, forming a sandwich structure (Scheme 1). The electrochemical detection was performed to achieve the analysis of mimetic exosomes. To the best of our knowledge, this is the first time to develop double imprinting-based detection method for determining the particle size distribution, providing an effective way to analyze the complicated biosamples.

2. Experimental section

2.1. Preparation of SiO_2@Ag/MPBA probe

SiO_2 NPs are synthesized according to the methods reported in Zhang's group, and details are given in the supplementary information [29]. Then, 1 mg/mL SiO_2 NPs with 50 nm in diameter dispersed into ultrapure water was quickly added into 10 mL of 1.18 mM freshly prepared $[Ag(NH_3)_2]^+$ solution, followed by the shaking at 25 °C for 1 h to adsorb Ag^+ onto the surface of SiO_2 NPs. Subsequently, the above solution was mixed with 50 mL of ethanol solution containing 50 mM PVP, and continuously stirred for another 7 h at 72 °C. The precipitate obtained by centrifugation was washed three times with ethanol absolute, and then dispersed into 10 mL of ethanol absolute. Afterwards, 200 μL of 1.0 mM MPBA was added to 1 mL of above SiO_2@Ag solution, and shaken at 37 °C for 12 h. The obtained product was washed three times with absolute ethanol and ultrapure water, respectively, and then dispersed into 1 mL of 0.01 M phosphate buffer saline (PBS) (pH 7.4) to obtain SiO_2@Ag/MPBA probe.

2.2. Preparation of SiO_2@HRP

SiO_2@HRP were prepared by aldehyde crosslinking. First, 1 mg of SiO_2 was dispersed into 10 mL of ethanol absolute, and then 0.1 mL of 3-aminopropyltrimethoxysilane (APTMS) was rapidly added under continuous stirring. After reacting for 12 h at room temperature, the resulting solution was centrifuged and washed three times with ethanol absolute and ultrapure water, respectively. The amino-functionalized SiO_2 NPs were dispersed into 1 mL of 0.1 M PBS (pH 7.4), followed by the addition of 5 mL of 5% glutaraldehyde. The aldehyde-functionalized SiO_2 NPs were obtained by centrifugation and washed three times with 0.1 M PBS (pH 7.4) after shaking at 37 °C for 2 h. 100 μL of 1 mg/mL HRP was added to 1 mL of the above aldehyde-functionalized SiO_2 NPs-dispersed PBS (0.1 M, pH 7.4) solution. The mixture was shaken at 37 °C for 12 h, and then centrifuged and treated with 0.1 M PBS (pH 7.4). Finally, SiO_2@HRP were obtained in 0.1 M PBS (pH 7.4). The preparation process of SiO_2@BSA and SiO_2@chitosan NPs [30] were the same except that the concentration of chitosan was changed to 2% (w/v).

2.3. Fabrication of the double-imprinting polymers

Au NPs-GO was prepared according to the methods previously reported by Zhang's group [29], and the details were shown in the supplementary information. First, the glassy carbon electrode was polished with 1.0 and 0.05 μm aluminum powder, and then rinsed with ethanol absolute and ultrapure water, respectively. After dried by the nitrogen, 5 μL of 0.1% chitosan solution was dropped on the surface of the treated electrode, and dried in the air. Then, 5 μL of Au NPs-GO solution (1 mg/mL) was added dropwise and allowed to air dry. Subsequently, the modified electrode was immersed in 200 μM MPBA ethanol solution for 6 h to bond and fix template-SiO_2@HRP, followed by washing with ethanol absolute and ultrapure water. To form a molecularly imprinted membrane, 5 μL of SiO_2@HRP in PBS (0.1 M, pH 8.0) was added dropwise to the modified surface and incubated for 30 min at 37 °C. After washing the electrode three times with 0.1 M PBS (pH 8.0), 5 μL of prepolymer containing 2.0 mM 4-vinylphenylboronic (VPBA), 1.0 mM methacrylic acid (MAA), 5.0 mM 2,2-azobisisobutyronitrile (AIBN) and 1.0 mM ethylene glycol dimethacrylate (EGDMA) was dropped on the surface, and incubated at room temperature for 12 h. Since the affinity between the DIP film and the template could be sharply reduced with the sodium dodecyl sulfate (SDS) by denaturing the protein and the hydrolysis of boric acid ester in

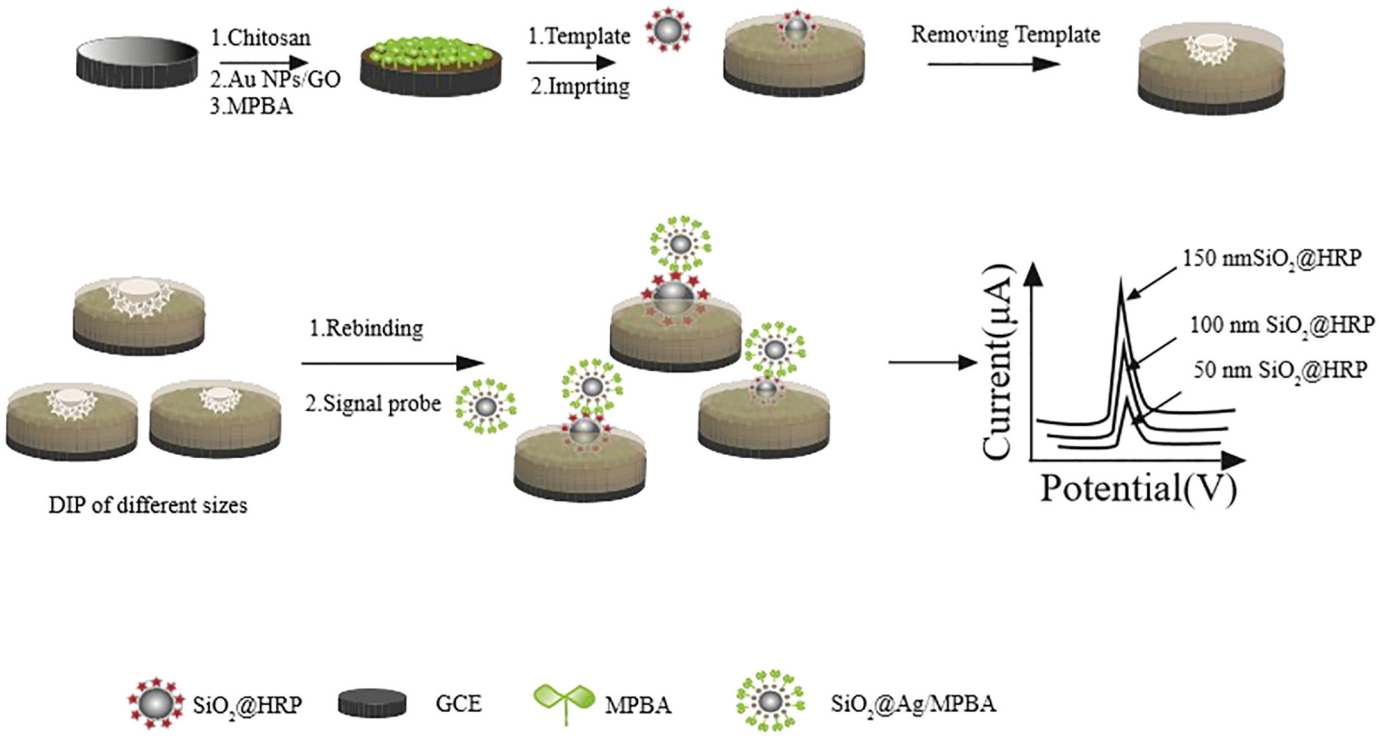

Scheme 1. Schematic illustration of the particle size distribution detection based on double-imprinting.

acid [31], the template was then eluted with 0.1 M HCl containing 10% SDS (w/v), obtaining the DIP-modified electrode. Non-imprinted polymers (NIP) covered electrode without template molecules was prepared under the same conditions for comparison.

2.4. Electrochemical detection with DIP film

5 μL of SiO_2@HRP solution in 100 mM PBS (pH 7.4) was added to each DIP modified electrode, followed by incubation at 37 °C for 45 min. Then, the modified electrode was rinsed with acetonitrile-water solution (3:7, v/v) for 6 min. The following incubation with 5 μL of SiO_2@Ag/MPBA was performed for 10 min at 37 °C. After gently washing with acetonitrile-10 mM PBS (pH 9.0, 3:7, v/v) for 6 min, the obtained electrode was detected using differential pulse voltammetry (DPV) in 0.1 M PBS (pH 7.4). The pulse amplitude, pulse period and pulse width of DPV were set as 50 mv, 0.2 s and 50 ms, respectively.

3. Results and discussion

3.1. Characterization of SiO_2 NPs, SiO_2@Ag/MPBA probe and double imprinting films

The characterization of SiO_2 NPs at different sizes is shown in supplementary information (Fig. S1). Since boric acid can bind to glycosyl groups on glycoproteins, MPBA-modified SiO_2@Ag was used here to label the captured targets. To confirm the successful synthesis of SiO_2@Ag/MPBA, TEM (Fig. 1) and UV–vis spectra (Fig. S2) were employed. As shown in Fig. 1, the pure monodisperse silica NPs are spherical and have a smooth surface with an average diameter of 90 nm. After coated with Ag NPs, the surface of the SiO_2 NPs became rougher due to the adhesion of a large amount of small-sized Ag NPs, and the size of SiO_2@Ag is slightly larger than the naked SiO_2, indicating the formation of SiO_2@Ag NPs. To verify the successful modification of MPBA, UV–vis spectra was used (Fig. S2). Due to the presence of the benzene ring, MPBA has an ultraviolet absorption peak at 250 nm. While, there is no significant absorption at 250 nm for SiO_2@Ag NPs except the absorption of Ag NPs at 450 nm. Therefore, the peaks at 250 nm and 450 nm are simultaneously observed in the spectra of SiO_2@Ag/MPBA, indicating the successful modification of MPBA.

The boronate affinity DIPs was characterized by AFM and FT-IR (Fig. S3). AFM was employed to characterize DIP and NIP films. Fig. 2 shows the AFM images of DIPs prepared using SiO_2@HRP with ~50 nm (Fig. 2A), ~100 nm (Fig. 2B) and ~150 nm (Fig. 2C) in diameter as template. The formed uniform cavities are located on the surface of the imprinting film and the sizes are consistent with those of template molecules. While, the NIP film (Fig. 2D) has a smooth surface, which is significantly different from the DIP film without the templates, indicating the successful preparation of boronic acid-affinity DIP films.

3.2. Electrochemical characterization of the DIP film

Cyclic voltammetry (CV) and electrochemical impedance spectroscopy (EIS) were performed to characterize the modification process of electrode surface in 5 mM $K_3[Fe(CN)_6]/K_4[Fe(CN_6)]$ solution containing 0.1 M KCl. As observed from Fig. 3A, after modification of Au NPs-GO, the redox current intensity (green curve) is higher than that of GCE (yellow curve), which is attributed to the larger specific surface area and better conductivity of Au NPs-GO. The peak current of DIP before removal of template (red curve) drops sharply, probably due to the fact that the polymer film and template molecules greatly hinder the electron conduction. While, the removal of the template enhances the peak current (blue curve), because the imprinted cavities reduce the transport barrier of $[Fe(CN)_6]^{3-/4-}$ to the electrode surface. After incubation with the target – SiO_2@HRP (Fig. S4), the peak current intensity is declined (magenta curve), indicating the successful rebinding of targets on the imprinted film. The electrochemical impedance spectroscopy (EIS) shows the consistent results with the CV curves (Fig. 3B). The inner illustration is the equivalent circuit diagram, consisting of the solution impedance (R_s), electronic transfer impedance (R_{et}), the constant phase (Q_{dl}) and the Warburg impedance element (W) [32]. Clearly, the modification of Au NPs-GO on the surface (green dots) makes the electronic transfer impedance (R_{et}) decreased compared with the bare GCE (yellow dots). When the surface of the Au NPs-GO/GCE is wrapped with DIP film (red dots), the value of R_{et} is increased to 1000 Ω due to the weak conductivity of the film with the template. Then, it is greatly reduced after removing the template (blue dots), which demonstrates that the imprinted cavity enhances the electron transport properties of DIPs film. The incubation with the targets causes another increase of R_{et} (magenta curve), but the value is smaller than that of DIP before elution, probably due to the non-occupation of partial cavities on the film, providing a pathway for electron conduction. The impedance data were then fitted with the proposed equivalent circuit by ZSimpWin software (Fig. S5), and $\chi^2 \leq 2.3053 \times 10^{-3}$ (χ^2 is the residual sum of squares between the fitted data and the experimental data) reveals the good *consistency*.

The ability of DIP film to rebind the target – SiO_2@HRP was then investigated with SiO_2@Ag/MPBA. After the incubation of with 100 nm SiO_2@HRP (2.89×10^7 particles/mL), the DPV signals were collected at different modified electrodes. As shown in Fig. 4, Au NPs-GO modified electrode produces extremely weak current response (black curve, $I = 0.207$ μA). After modifying the NIP film, a stronger electrochemical signal was generated (blue curve, $I = 0.678$ μA), because a small amount of the targets was

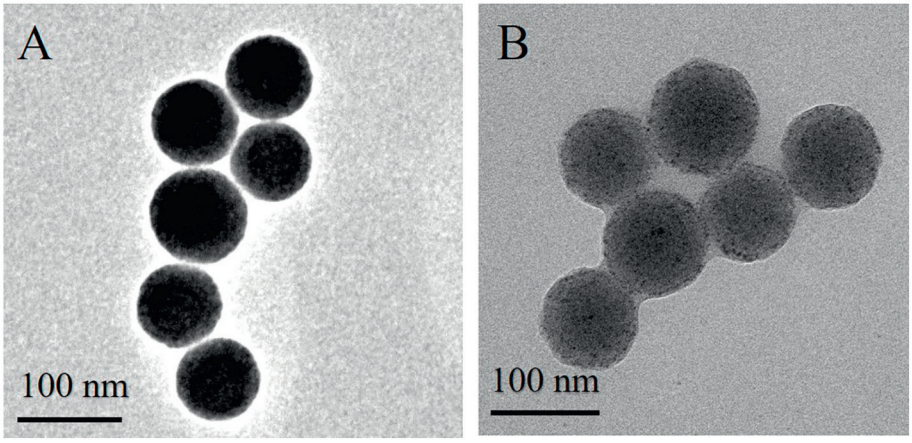

Fig. 1. TEM images of (A) SiO_2 and (B) SiO_2@Ag.

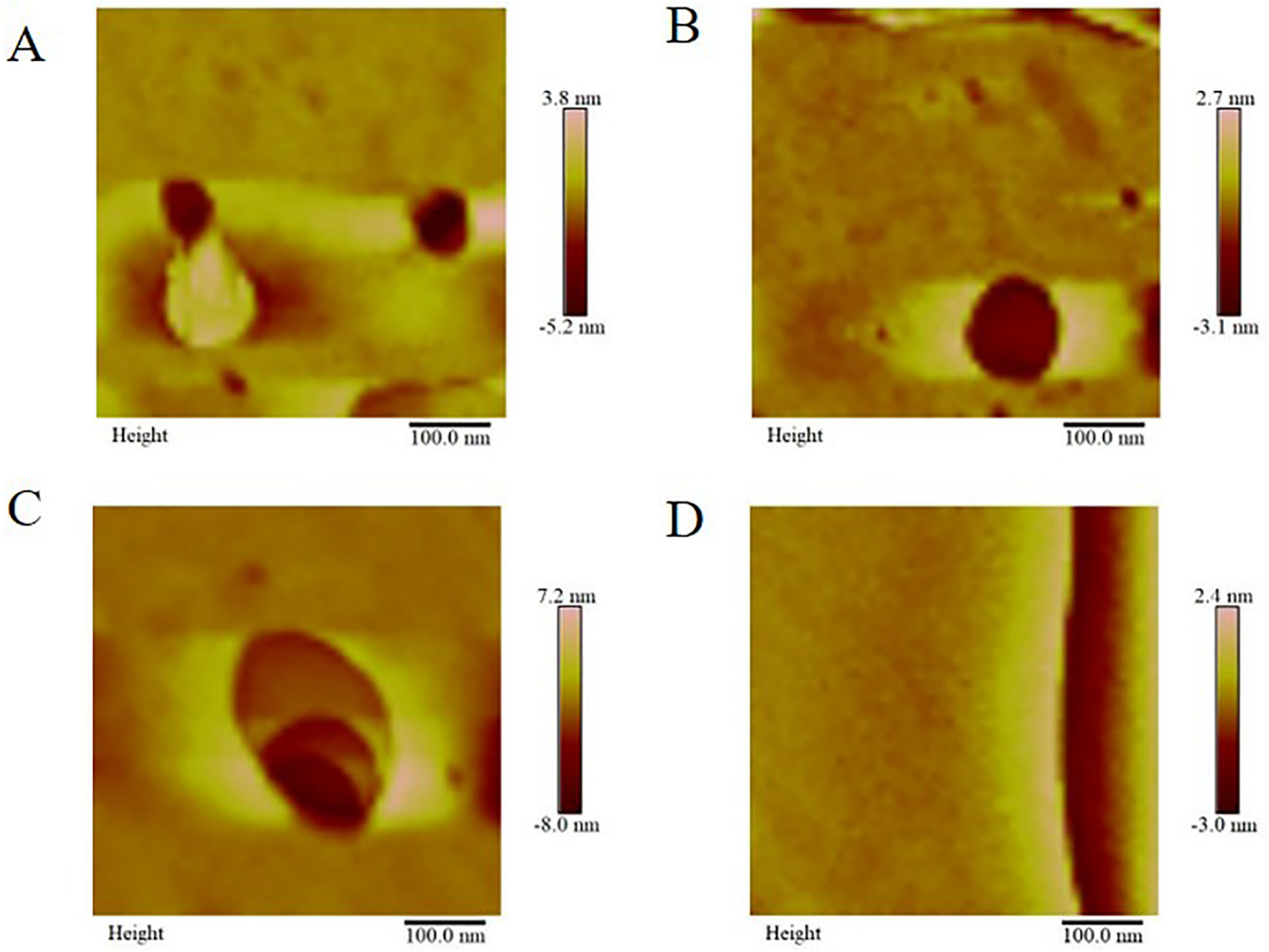

Fig. 2. AFM images of DIP films after removal of SiO_2@HRP with the diameter in (A) 50 nm, (B) 100 nm and (C) 150 nm, and (D) NIP film.

adsorbed due to the presence of exposed boric acid groups on the polymer surface. For DIP film, the removal of the template molecule generated lots of cavities with the matched size to capture the targets, exhibiting much stronger signal (magenta dots, I = 2.209 μA). While, the DIP film without targets shows a much weakened DPV response in PBS (red dots, I = 0.625 μA), due to the adsorption of few signal molecules. Obviously, the DIP films exhibit more affinity towards targets.

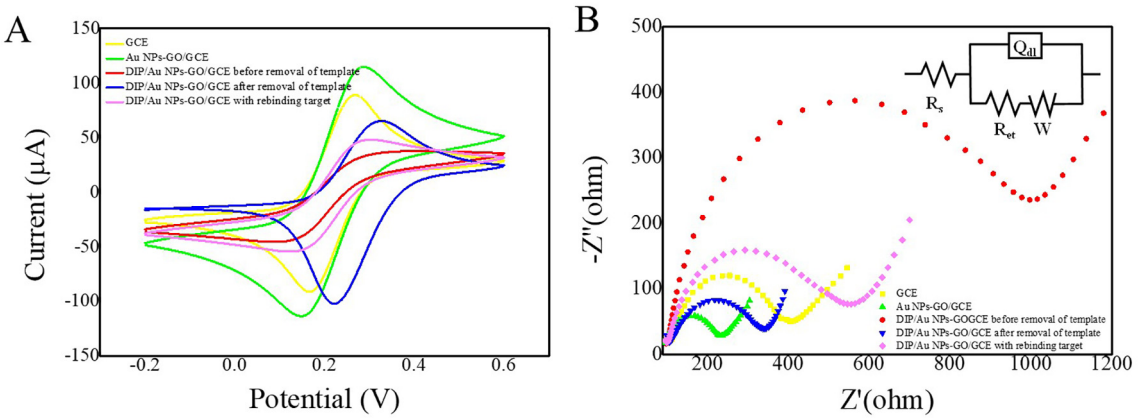

Fig. 3. CV (A) and EIS (B) of GCE (yellow), Au NPs-GO/GCE (green), DIP-Au NPs-GO/GCE before removal of the template (red), DIP-Au NPs-GO/GCE after removal of the template (blue), and DIP-Au NPs-GO/GCE with rebinding of SiO_2@HRP (magenta) in 5 mM $K_3[Fe(CN)_6]/K_4[Fe(CN_6)]$ solution containing 0.1 M KCl. Insert was the fitted Randles-equivalent circuit model.

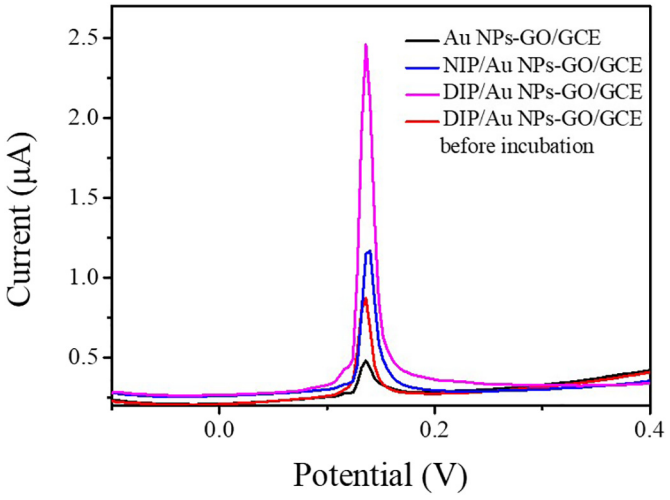

Fig. 4. DPV responses of (a) Au NPs-GO/GCE (black curve), NIP-Au NPs-GO/GCE (blue curve) and DIP-Au NPs-GO/GCE (magenta curve) in 0.1 mM PBS (pH 7.4) after incubating with 100 nm SiO_2@HRP (2.89×10^7 particles/mL) for 40 min, and DIP-Au NPs-GO/GCE in 0.1 M PBS (pH 7.4) before the incubation (red curve).

3.3. Double recognition of DIPs

Double imprinting was realized based on the size of SiO_2 NPs and the loaded proteins on the surface. In order to verify the necessity and feasibility of the DIPs, two kinds of interferents were prepared. The one is 100 nm SiO_2 NPs wrapped by BSA (without glycosyl) and polyglycol chiston, forming SiO_2@BSA and SiO_2@chitosan, respectively, and used to investigate the functional efficacy of proteins on the surface towards the selectivity of DIPs (Fig. 5A). It can be found that all of the interferents have electrochemical response compared to the blank, but they are much weaker than SiO_2@HRP at the same concentration. It indicates that non-glycoprotein or other glycoprotein-wrapped SiO_2 NPs could be captured few by DIP film, revealing that the surface morphology of the template molecules plays an important role in double imprinting.

The other is SiO_2@HRP at different sizes, and employed to evaluate the influence of template size on the selectivity of DIPs. A DIP film was prepared using 100 nm SiO_2@HRP as template, and then 50 nm, 100 nm and 150 nm SiO_2@HRP (10^7 particles/mL) were detected by the DIP film, respectively. As shown in Fig. 5B, the current signals of both 50 nm and 150 nm SiO_2@HRP are much smaller than that of 100 nm SiO_2@HRP, confirming that the prepared DIP film has the ideal size selection capability. While, NIP shows the similar affinity to the targets and interferents, caused by the nonspecific adsorption of the polymer membrane.

Obviously, the binding of target – SiO_2@HRP by the DIP film relies on the double match of the size and surface morphology. While, a single match couldn't realize the stable capture of the target by the film. This opens up the possibility to determine the particle size distribution of exosomes using this double imprinting technique.

3.4. Optimization of experimental conditions

In order to obtain the most excellent performance of the DIP-based sensor, some key experimental conditions were optimized using 50 nm SiO_2@HRP (2.38×10^9 particles/mL) as the template, including the concentration of MBPA, the ratio of two functional monomers MAA and VPBA during polymerization, pH of the incubation solution and the rebinding time of the target by DIP film.

As shown in Fig. 6A, the current intensity increases gradually with the increase of the MPBA concentration in the range of 100–200 μM, and then decreases as the concentration continues to increase, which may be attributed to excessive MPBA absorbed on the surface of electrode. Therefore, 200 μM MPBA was selected as the optimal modification concentration.

Since the imprinting layer formed by self-polymerization of a single VPBA monomer exhibits poor hydrophilic, MAA with the carboxyl group was introduced as another functional monomer to increase the hydrophilicity by the interaction with the amino group on the protein. The molar ratio of the two monomers directly affects the binding efficiency of the DIP film to the glycoprotein. It could be observed that when the molar ratio of MAA: VPBA varies from 2:1 to 1:2 (Fig. 6B), the signal gradually increases, indicating the enhanced binding ability of DIP film towards the target. Then, the current response decreases as the molar ratio changes from 1:2 to 1:4, since the content decrease of MAA results in the reduced adsorption ability of the DIP film. Consequently, the optimal molar ratio of the two functional monomers was 1:2.

The pH value of the incubation solution could affect the combination of boric acid and glycosyl cis diol in the prepolymer and then the analytical performance of the sensor. Thus, it was optimized and the results were shown in Fig. 6C. Clearly, the current signal increases in the pH range of 5–8, indicating the enhanced adsorption capacity of the DIP film towards the target. It reaches a maximum at pH = 8, and then it declines gradually, which reflecting that the slightly alkaline incubation solution facilitates adsorption of the target. Hence, pH 8 was chosen as the optimal value.

The rebinding time of the target by DIP films could also influence the detection sensitivity. Fig. 6D displays its effect on current response in the range of 10–50 min. It could be observed that 40 min of the incubation time generates a peak signal, and then the current reaches a plateau,

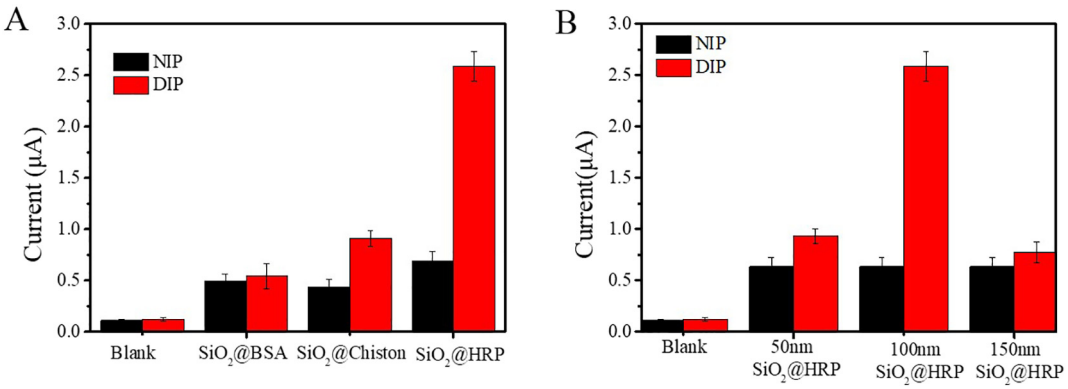

Fig. 5. Investigation of double selectivity by DIP and NIP films: (A) Current responses of SiO_2@BSA, SiO_2@Chiston and SiO_2@HRP (2.89×10^7particles/mL) in 0.1 M PBS (pH 7.4) with blank solution (0.1 M PBS, pH 7.4) as control; (B) Current responses of 50 nm, 100 nm and 150 nm SiO_2@HRP (2.89×10^7particles/mL) in 0.1 M PBS (pH 7.4). (n = 3, RSD ≤ 5%).

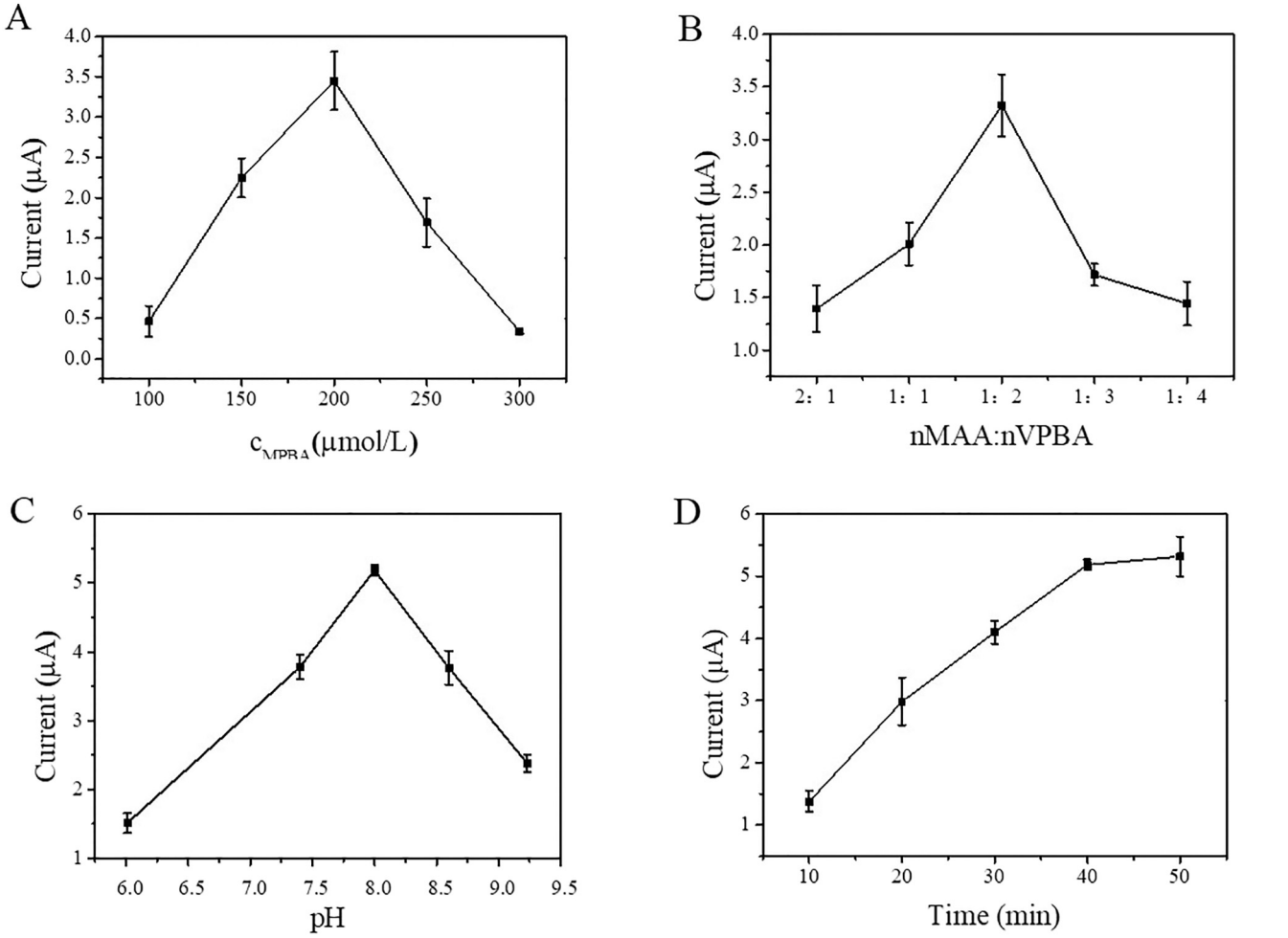

Fig. 6. Effect of (A) the concentration of MBPA, (B) the ratio of two functional monomers MAA and VPBA, (C) pH of the incubation solution and (D) the rebinding time of the target by DIP film on the analytical performance of DIP film.

indicating that the adsorption of the target by the DIP film is saturated. So, 40 min was set as the best rebinding time.

3.5. Analysis of particle size distribution of mimetic exosomes by the DIP films

HRP, a kind of glycoproteins with the advantage of good stability and easy access, was modified on the surface of SiO_2 NPs to construct mimetic exosomes - SiO_2@HRP. It is similar to exosomes, both displaying spherical nanoparticles coated by large amounts of glycoproteins. Meanwhile, SiO_2@HRP is size-controllable, thus its mixture could be obtained at a PSD similar to that of exosomes. Besides, it is a kind of solid nanoparticles, and could be employed as templates to form a series of imprinted films to capture the targets. Exosomes are non-uniform vesicles with about 30–150 nm in diameter, but random PSD [33–35]. According to the PSD of exosomes extracted from SK-BR-3 cells detected by NTA (Fig. S6), they are mainly concentrated around 100–150 nm. Considering those smaller particles, 50 nm SiO_2@HRP, 100 nm SiO_2@HRP and 150 nm SiO_2@HRP were selected as the representative NPs to build the PSD analysis model.

In order to investigate the particle size distribution of the mimetic exosomes, the DIP films were prepared separately with 50 nm SiO_2@HRP (DIP-50 for short), 100 nm SiO_2@HRP (DIP-100 for short) and 150 nm SiO_2@HRP as template (DIP-150 for short), followed by recording the current responses of DIP-50 to 50 nm SiO_2@HRP, DIP-100 to 100 nm SiO_2@HRP and DIP-150 to 150 nm SiO_2@HRP at different concentrations. As shown in Fig. 7A, C and E, the current intensities were enhanced as the target concentration increases. To eliminate the influence of the nonspecific absorption, the calibrated currents ($\Delta I = I_{DIP} - I_{NIP}$) were employed for the analysis. The linear correlations between the current intensity and the logarithm of the concentration were deduced as $\Delta I_{50} = -1.52 + 0.50 \times \lg c_{50}$ ($R^2 = 0.998$ in the range of 2.38×10^4–2.38×10^9 particles/mL), $\Delta I_{100} = -1.61 + 0.48 \times \lg c_{100}$ ($R^2 = 0.998$ in the range of 2.89×10^4–2.89×10^9 particles/mL) and $\Delta I_{150} = -1.54 + 0.49 \times \lg c_{150}$ ($R^2 = 0.998$ in the range of 5.75×10^4–5.75×10^9 particles/mL) with the limit of detection of 1.44×10^3 particles/mL, 5.68×10^2 particles/mL and 7.70×10^2 particles/mL, respectively (Fig. 7B, D and F). Using these calibration curves, the particle size distribution of mixed SiO_2@HRP were analyzed. The mixing ratio was selected as 50 nm:100 nm:150 nm = 5.0%:42.5%:52.5%, referring to the particle size distribution of exosomes from SK-BR-3 breast cancer cells detected by NTA. Thus, the mixed SiO_2@HRP could be regarded as mimetic exosomes. Then, the detection was performed with DIP-50, DIP-100 and DIP-150, respectively, obtaining a ratio of 50 nm:100 nm:150 nm = 3.6%:43.0%:53.4% (Fig. 7G). The relative concentration errors between DIP and NTA were calculated according to the equation of $R = \frac{C_{DIP} - C_{NTA}}{C_{NTA}} \times 100\%$ [36], obtaining 1.7%, 7.6% and 6.7%, for 50 nm, 100 nm and 150 nm SiO_2@HRP, respectively (Fig. 7H). Clearly, this similarity reveals that the DIP film has the excellent performance in determining the particle size distribution of mixed particles.

The analytical performance of the DIP film was further compared with other reported methods in terms of the capability to determine the particle size distribution (PSD), morphology (including the shape and surface ultrastructure) and concentration of nanoparticles, which are the main physical and structural information of exosomes, and also the measurement time

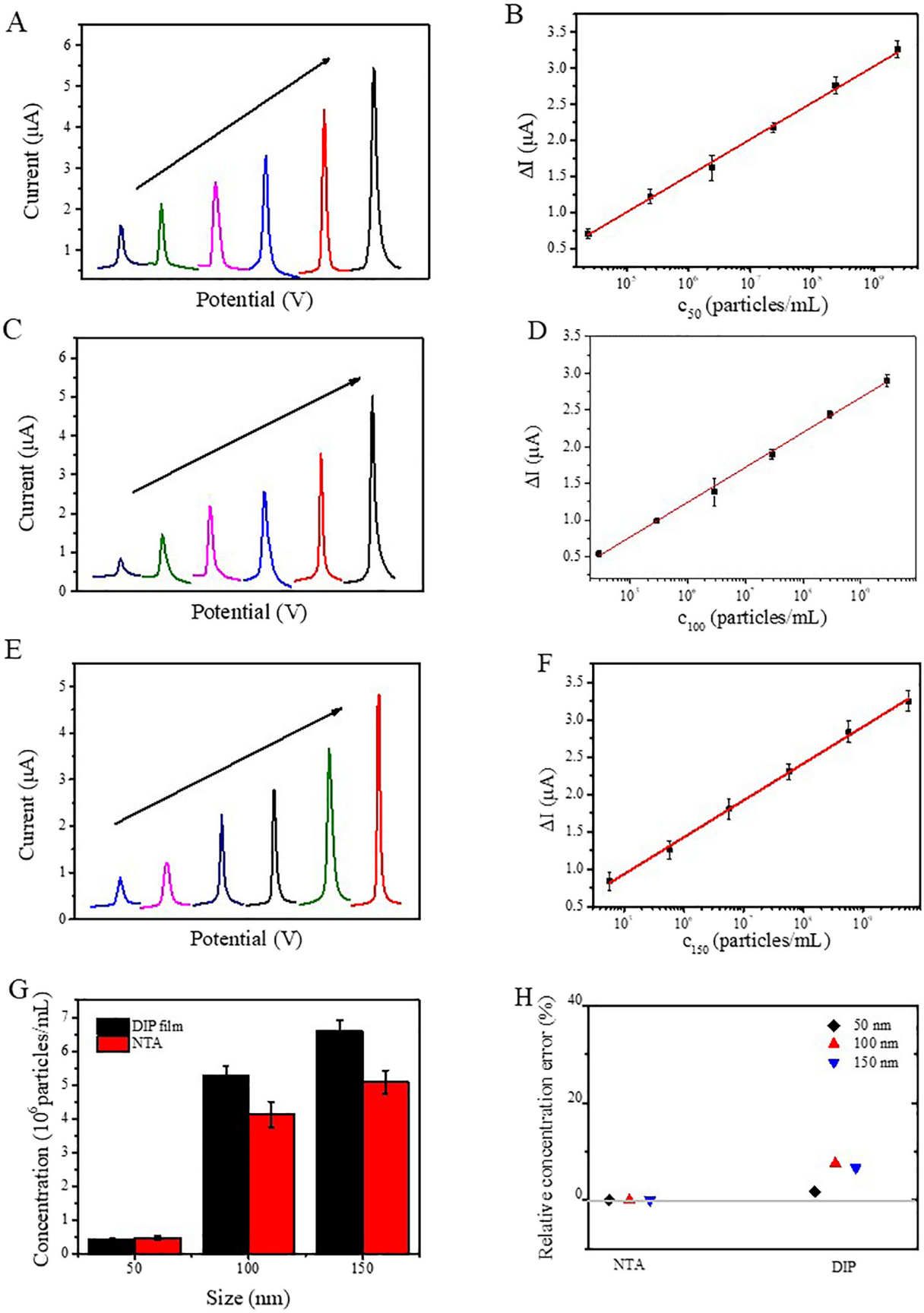

Fig. 7. DPV curves and the corresponding linear correlations between the current intensity and the logarithm of the concentration of (A and B) 50 nm SiO_2@HRP in the range of 2.38×10^4–2.38×10^9 particles/mL, (C and D) 100 nm SiO_2@HRP in the range of 2.89×10^4–2.89×10^9 particles/mL, and (E and F) 150 nm SiO_2@HRP at different concentrations in the range of 5.75×10^4–5.75×10^9 particles/mL, detected by DIP-50, DIP-100 and DIP-150, respectively. (G) Ratio of mimetic exosomes detected by DIP film and NTA method (n = 3). (H) Relative concentration errors between DIP and NTA for 50 nm (black diamond), 100 nm (red triangle) and 150 nm SiO_2@HRP (blue triangle).

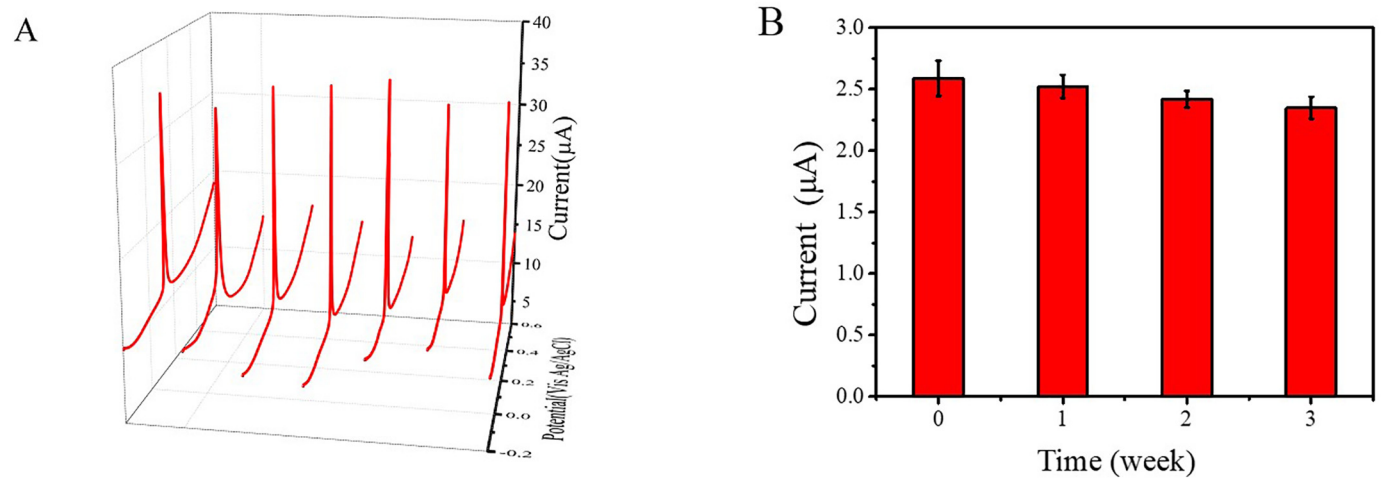

Fig. 8. (A) DPV curves SiO_2@HRP (2.89 × 10^7 particles/mL) at seven DIP-100-modified electrodes; (B) Peak current of SiO_2@HRP (2.89 × 10^7 particles/mL) detected by DIP-100-modified electrode per 7 days.

(Table S1). Clearly, this developed DIP film displays an excellent performance, and could provide all the information of particle size distribution, concentration and morphology. Besides, it does not need too much measurement time.

3.6. Reproducibility and stability of DIP films

The DIP-100-modified electrodes (n = 7) prepared under the same conditions were used to investigate the reproducibility of DIP film with the detection of 100 nm SiO_2@HRP (2.89 × 10^7 particles/mL, Fig. 8A). The relative standard deviation (RSD) of the current responses was calculated as 8.2%, indicating the excellent reproducibility. To test the stability of DIP film, the DIP-100-modified electrode was stored at 4 °C for 3 weeks and used to detect 100 nm SiO_2@HRP (2.89 × 10^7 particles/mL) every week. It could be found that the current signal remains 90.7% of the initial value after 3 weeks (Fig. 8B), presenting the superior stability of DIP films.

4. Conclusions

In summary, double imprinting films were developed to analyze the particle size distribution of mimetic exosomes – SiO_2@HRP at mixed sizes (50 nm, 100 nm and 150 nm), depending on both the size of SiO_2 NPs and the morphology of protein – HRP modified on the surface. Using SiO_2@Ag/MPBA as signal tag, the DIP film could recognize 50 nm, 100 nm and 150 nm SiO_2@HRP in linear ranges of 2.89 × 10^4–2.89 × 10^9 particles/mL, 2.89 × 10^4–2.89 × 10^9 particles/mL and 5.75 × 10^4–5.75 × 10^9 particles/mL with the limit of detection of 1.44 × 10^3 particles/mL, 5.68 × 10^2 particles/mL and 7.70 × 10^2 particles/mL, respectively. Based on the deduced linear correlations, the particle size distribution of mimetic exosomes with the mixing ratio referring to that of exosomes from cells detected by NTA was analyzed, obtaining a similar result with small relative concentration errors of 1.7%, 7.6% and 6.7%, for 50 nm, 100 nm and 150 nm SiO_2@HRP, respectively. Moreover, the DIP film exhibited excellent reproducibility and stability.

Using this the double recognition-based method, the interference of liposomes and protein aggregates with similar size and shape could be eliminated in the real analysis. It could be applied to the separation and detection of exosomes in the future, and the further analysis of exosomes for early diagnosis of cancers by varying the modified proteins on the surface of the nanoparticles. Besides, this fabricated DIP film could be integrated in the portable devices, facilitating point-of-care testing and home healthy diagnosis.

CRediT authorship contribution statement

Yuyuan Zhu: Conceptualization, Formal analysis, Investigation, Writing - original draft.**Yu An:**Investigation, Formal analysis.**Rui Li:**Validation.**Fan Zhang:**Resources, Writing - review & editing.**Qingjiang Wang:** Resources, Writing - review & editing.**Pingang He:**Resources, Writing - review & editing

Declaration of competing interest

The authors declare that they have no known competing financial interests or personal relationships that could have appeared to influence the work reported in this paper.

Acknowledgments

This work was financially supported by the National Natural Science Foundation of China (Grant No. 21575042).

Appendix A. Supplementary data

Supplementary data to this article can be found online at https://doi.org/10.1016/j.jelechem.2020.113969.

References

[1] G. Raposo, W. Stoorvogel, Extracellular vesicles: exosomes, microvesicles, and friends, J. Cell Biol. 200 (2013) 373–383.
[2] Y. Weng, Z. Sui, Y. Shan, Y. Hu, Y. Chen, L. Zhang, Y. Zhang, Effective isolation of exosomes with polyethylene glycol from cell culture supernatant for in-depth proteome profiling, Analyst 141 (2016) 4640–4646.
[3] Y. Naito, Y. Yoshioka, Y. Yamamoto, T. Ochiya, How cancer cells dictate their microenvironment: present roles of extracellular vesicles, Cell. Mol. Life Sci. 74 (2017) 697–713.
[4] H. Vallhov, C. Gutzeit, S.M. Johansson, N. Nagy, M. Paul, Q. Li, S. Friend, T.C. George, E. Klein, A. Scheynius, Exosomes containing glycoprotein 350 released by EBV-transformed B cells selectively target B cells through CD21 and block EBV infection in vitro, J. Immunol. 186 (2011) 73–82.
[5] S. Chauhan, S. Danielson, V. Clements, N. Edwards, S. Ostrand-Rosenberg, C. Fenselau, Surface glycoproteins of exosomes shed by myeloid-derived suppressor cells contribute to function, J. Proteome Res. 16 (2016) 238–246.
[6] C. Emanueli, A.I. Shearn, G.D. Angelini, S. Sahoo, Exosomes and exosomal miRNAs in cardiovascular protection and repair, Vasc. Pharmacol. 71 (2015) 24–30.
[7] E. van der Pol, A.G. Hoekstra, A. Sturk, C. Otto, T.G. van Leeuwen, R. Nieuwland, Optical and non-optical methods for detection and characterization of microparticles and exosomes, J. Thromb and Haemost 8 (2010) 2596–2607.
[8] J. Conde-Vancells, E. Rodriguez-Suarez, N. Embade, D. Gil, R. Matthiesen, M. Valle, F. Elortza, S.C. Lu, J.M. Mato, J.M. Falcon-Perez, Characterization and comprehensive proteome profiling of exosomes secreted by hepatocytes, J. Proteome Res. 7 (2008) 5157–5166.

[9] R.A. Dragovic, C. Gardiner, A.S. Brooks, D.S. Tannetta, D.J. Ferguson, P. Hole, B. Carr, C.W. Redman, A.L. Harris, P.J. Dobson, P. Harrison, I.L. Sargent, Sizing and phenotyping of cellular vesicles using nanoparticle tracking analysis, Nanomedicine: NBM 7 (2011) 780–788.
[10] V. Filipe, A. Hawe, W. Jiskoot, Critical evaluation of nanoparticle tracking analysis (NTA) by NanoSight for the measurement of nanoparticles and protein aggregates, Pharm. Res. 27 (2010) 796–810.
[11] J. Gross, S. Sayle, A.R. Karow, U. Bakowsky, P. Garidel, Nanoparticle tracking analysis of particle size and concentration detection in suspensions of polymer and protein samples: influence of experimental and data evaluation parameters, Eur. J. Pharm. Biopharm. 104 (2016) 30–41.
[12] B. Vestad, A. Llorente, A. Neurauter, S. Phuyal, B. Kierulf, P. Kierulf, T. Skotland, K. Sandvig, K.B.F. Haug, R. Ovstebo, Size and concentration analyses of extracellular vesicles by nanoparticle tracking analysis: a variation study, J. Extracell Vesicles 6 (2017), 1344087.
[13] C. Gardiner, Y.J. Ferreira, R.A. Dragovic, C.W. Redman, I.L. Sargent, Extracellular vesicle sizing and enumeration by nanoparticle tracking analysis, J Extracell Vesicles 2 (2013).
[14] R.A. Dragovic, G.P. Collett, P. Hole, D.J. Ferguson, C.W. Redman, I.L. Sargent, D.S. Tannetta, Isolation of syncytiotrophoblast microvesicles and exosomes and their characterisation by multicolour flow cytometry and fluorescence nanoparticle tracking analysis, Methods 87 (2015) 64–74.
[15] Y. Yuana, T.H. Oosterkamp, S. Bahatyrova, B. Ashcroft, P. Garcia Rodriguez, R.M. Bertina, S. Osanto, Atomic force microscopy: a novel approach to the detection of nanosized blood microparticles, J. Throm. Haemost 8 (2010) 315–323.
[16] E.N. Nolte-'t Hoen, E.J. van der Vlist, M. Aalberts, H.C. Mertens, B.J. Bosch, W. Bartelink, E. Mastrobattista, E.V. van Gaal, W. Stoorvogel, G.J. Arkesteijn, M.H. Wauben, Quantitative and qualitative flow cytometric analysis of nanosized cell-derived membrane vesicles, Nanomedicine NBM 8 (2012) 712–720.
[17] V. Pospichalova, J. Svoboda, Z. Dave, A. Kotrbova, K. Kaiser, D. Klemova, L. Ilkovics, A. Hampl, I. Crha, E. Jandakova, L. Minar, V. Weinberger, V. Bryja, Simplified protocol for flow cytometry analysis of fluorescently labeled exosomes and microvesicles using dedicated flow cytometer, J. Extracell Vesicles 4 (2015) 25530.
[18] K. Witwer, E. Buzás, L. Bemis, A. Bora, C. Lässer, J. Lötvall, E. Hoen, M. Piper, S. Sivaraman, J. Skog, C. Théry, M. Wauben, F. Hochberg, Standardization of sample collection, isolation and analysis methods in extracellular vesicle research, J. Extracell Vesicles 2 (2013) 20360.
[19] W. Anderson, D. Kozak, V.A. Coleman, A.K. Jamting, M. Trau, A comparative study of submicron particle sizing platforms: accuracy, precision and resolution analysis of polydisperse particle size distributions, J. Colloid Interf. Sci 405 (2013) 322–330.
[20] G. Wulff, Use of polymers with enzyme-analogous structures for the resolution of racemates, Angew Chem. Int. Edit 11 (1972) 341.
[21] G. Vlatakis, L.I. Andersson, R. Müller, K. Mosbach, Drug assay using antibody mimics made by molecular imprinting, Nature 361 (1993) 645.
[22] W. Wan, M. Biyikal, R. Wagner, B. Sellergren, K. Rurack, Fluorescent sensory microparticles that 'light-up' consisting of a silica core and a molecularly imprinted polymer (MIP) shell, Angew Chem. Int. Edit 52 (2013) 7023–7027.
[23] F. Canfarotta, A. Poma, A. Guerreiro, S. Piletsky, Solid-phase synthesis of molecularly imprinted nanoparticles, Nat. Protoc. 11 (2016) 443.
[24] J. Wackerlig, R. Schirhagl, Applications of molecularly imprinted polymer nanoparticles and their advances toward industrial use: a review, Anal. Chem. 88 (2015) 250–261.
[25] L. Chen, X. Wang, W. Lu, X. Wu, J. Li, Molecular imprinting: perspectives and applications, Chem. Soc. Rev. 45 (2016) 2137–2211.
[26] J. Pan, W. Chen, Y. Ma, G. Pan, Molecularly imprinted polymers as receptor mimics for selective cell recognition, Chem. Soc. Rev. 47 (2018) 5574–5587.
[27] A. Hoshino, B. Costa-Silva, T.L. Shen, G. Rodrigues, A. Hashimoto, M. Tesic Mark, H. Molina, S. Kohsaka, A. Di Giannatale, S. Ceder, S. Singh, C. Williams, N. Soplop, K. Uryu, L. Pharmer, T. King, L. Bojmar, A.E. Davies, Y. Ararso, T. Zhang, H. Zhang, J. Hernandez, J.M. Weiss, V.D. Dumont-Cole, K. Kramer, L.H. Wexler, A. Narendran, G.K. Schwartz, J.H. Healey, P. Sandstrom, K.J. Labori, E.H. Kure, P.M. Grandgenett, M.A. Hollingsworth, M. de Sousa, S. Kaur, M. Jain, K. Mallya, S.K. Batra, W.R. Jarnagin, M.S. Brady, O. Fodstad, V. Muller, K. Pantel, A.J. Minn, M.J. Bissell, B.A. Garcia, Y. Kang, V.K. Rajasekhar, C.M. Ghajar, I. Matei, H. Peinado, J. Bromberg, D. Lyden, Tumour exosome integrins determine organotropic metastasis, Nature 527 (2015) 329–335.
[28] P. Li, M. Kaslan, S.H. Lee, J. Yao, Z. Gao, Progress in exosome isolation techniques, Theranostics 7 (2017) 789–804.
[29] M. You, S. Yang, W. Tang, F. Zhang, P.G. He, Ultrasensitive electrochemical detection of glycoprotein based on boronate affinity sandwich assay and signal amplification with functionalized SiO_2@Au nanocomposites, ACS Appl. Mater. Inter 9 (2017) 13855–13864.
[30] R. Cao, D. Duan, L. Jiang, Z. Lu, F. Bao, K. Zheng, J. Li, Polysaccharide-coated beads platform for biomolecule analysis: evolution of SiO_2-based suspension arrays, Carbohyd. Polym 83 (2011) 818–823.
[31] X. Pang, G. Cheng, R. Li, S. Lu, Y. Zhang, Bovine serum albumin-imprinted polyacrylamide gel beads prepared via inverse-phase seed suspension polymerization, Anal. Chi. Acta 550 (2005) 13–17.
[32] M.C. Rodriguez, A.-N. Kawde, J. Wang, Aptamer biosensor for label-free impedance spectroscopy detection of proteins based on recognition-induced switching of the surface charge, Chem. Commun. (34) (2005) 4267–4269.
[33] R.E. Lane, D. Korbie, W. Anderson, R. Vaidyanathan, M. Trau, Analysis of exosome purification methods using a model liposome system and tunable-resistive pulse sensing, Sci. Rep. 5 (2015) 7639.
[34] V. Sokolova, A.K. Ludwig, S. Hornung, O. Rotan, P.A. Horn, M. Epple, B. Giebel, Characterisation of exosomes derived from human cells by nanoparticle tracking analysis and scanning electron microscopy, Colloids and Surface B 87 (2011) 146–150.
[35] H.W. King, M.M. Z., G.J. M., Hypoxic enhancement of exosome release by breast cancer cells, BMC Cancer 12 (2012) 421–430.
[36] E. van der Pol, F.A. Coumans, A.E. Grootemaat, C. Gardiner, I.L. Sargent, P. Harrison, A. Sturk, T.G. van Leeuwen, R. Nieuwland, Particle size distribution of exosomes and microvesicles determined by transmission electron microscopy, flow cytometry, nanoparticle tracking analysis, and resistive pulse sensing, J. Throm. Haemost 12 (2014) 1182–1192.